Advances in Applied Mathematics and Mechanics
Adv. Appl. Math. Mech., Vol. **8**, No. 6, pp. 953-970

DOI: 10.4208/aamm.2015.m1043
December 2016

Stability Analysis of a Fully Coupled Implicit Scheme for Inviscid Chemical Non-Equilibrium Flows

Yu Wang, Jinsheng Cai and Kun Qu*

National Key Laboratory of Science and Technology on Aerodynamic Design and Research, Northwestern Polytechnical University, Xi'an 710072, China

Received 21 April 2015; Accepted (in revised version) 13 October 2015

Abstract. Von Neumann stability theory is applied to analyze the stability of a fully coupled implicit (FCI) scheme based on the lower-upper symmetric Gauss-Seidel (LU-SGS) method for inviscid chemical non-equilibrium flows. The FCI scheme shows excellent stability except the case of the flows involving strong recombination reactions, and can weaken or even eliminate the instability resulting from the stiffness problem, which occurs in the subsonic high-temperature region of the hypersonic flow field. In addition, when the full Jacobian of chemical source term is diagonalized, the stability of the FCI scheme relies heavily on the flow conditions. Especially in the case of high temperature and subsonic state, the CFL number satisfying the stability is very small. Moreover, we also consider the effect of the space step, and demonstrate that the stability of the FCI scheme with the diagonalized Jacobian can be improved by reducing the space step. Therefore, we propose an improved method on the grid distribution according to the flow conditions. Numerical tests validate sufficiently the foregoing analyses. Based on the improved grid, the CFL number can be quickly ramped up to large values for convergence acceleration.

AMS subject classifications: 65M12, 65F10, 76K05

Key words: Stability, LU-SGS, non-equilibrium flows, Euler equations, flux Jacobian, grid refinement.

1 Introduction

The numerical computation of hypersonic flow fields has received increasing attention with the development of hypersonic vehicles. High-temperature effects [1] and multiple time scales make it difficult to compute hypersonic flow fields, especially non-equilibrium flows.

*Corresponding author.
Email: wangyu@mail.nwpu.edu.cn (Y. Wang), kunqu@nwpu.edu.cn (K. Qu), caijsh@nwpu.edu.cn (J. S. Cai)

One of the difficulties encountered in solving non-equilibrium flows is the "stiffness problem" [2]. That is, the chemical source term in the species equations is sometimes excessively large compared to the convective terms. Non-equilibrium effect results in a large difference between the time scales of the chemical reaction and the fluid dynamics, making it very difficult to determine an appropriate time step or CFL number. Inappropriate treatment of the stiffness problem results in a non-physical solution or divergent numerical solutions.

There are currently two approaches to dealing with the stiffness problem. In the first approach, the gas dynamic equations (i.e., the Navier-Stokes (NS) or Euler equations) and the species equations are solved separately and iteratively. This approach is called the "loosely coupled method" [3–5]. In the second approach, which is called the "coupled implicit method" [6–9, 25], the two sets of equations are solved simultaneously in a coupled implicit form. The loosely coupled method can be easily implemented but is numerically less stable than the coupled implicit method and is not well-suited for solving real-time problems. The coupled implicit method offers faster convergence and provides a better description of non-equilibrium effects. However, the coupled implicit method results in a complex, large block matrix system. The solution of such a large linear system requires large amounts of computer memory, especially when there is a large number of chemical species.

As a result of continuous improvements in computer performance and computing techniques, many of the difficulties of the coupled implicit method have been gradually overcome. Bussing [6] used the coupled point implicit method to solve the Euler equations for chemical non-equilibrium problems. Eberhardt [7] and Candler [8] separately used a fully coupled implicit (FCI) method, which is based on the LU-SGS and GSLR schemes, to solve the NS equations for thermochemical non-equilibrium problems. Spiegel [9, 10] also employed FCI method to solve the NS equations for chemical non-equilibrium problems using an unstructured hybrid grid.

However, alomost all of the numerical computations of non-equilibrium flows based on the coupled implicit method are limited by the time step or CFL number. To prevent a non-physical solution or divergent numerical solutions, a very small CFL number has been adopted in many studies [6–8], resulting in very slow convergence rate and long computing time. Moreover, setting the CFL number is an empirical and experimental exercise. From a mathematical perspective, for non-homogeneous nonlinear differential equation sets, if some of the source terms are positive or the Jacobian matrix of the source terms has positive eigenvalues, the equation sets have "growing" solutions [11], and numerical methods are unstable [12,13]. For general chemical kinetics, strong chemical reactions in non-equilibrium flows lead to dominant non-linear effects. In fact, even the fully coupled method faces robustness difficulties because of these effects [14]. Thus, the stability and convergence of the coupled implicit scheme must be specifically investigated to determine the effect of the chemical source term on numerical computations, and to determine a reasonable time step. At present, there is very little related theoretical research on the stability and convergence of the coupled implicit scheme. Venkateswaran [14] has

provided some brief conclusions on the stability of the FCI scheme.

In addition, the full Jacobian of chemical source term in the coupled implicit scheme requires the inversion of a large number of block matrices, which is highly time consuming and memory intensive. In particular, the advantage of "matrix-free" manipulation for the FCI scheme based on the LU-SGS method is lost. Thus, many researchers have used various diagonalized Jacobians to replace the full Jacobian. Kim [15] introduced a diagonal matrix that is formed from the diagonal terms of the full Jacobian. Eberhardt and Imlay [7] introduced a diagonal matrix in which the diagonal terms were set as the L_2 norm of each row of the full Jacobian. Ju [16] developed a more accurate diagonalized Jacobian by considering the chemical time scales of forward and backward reactions. Although these diagonalization methods can simplify computation, more research is needed to determine whether using the coupled implicit scheme with these diagonal matrices maintains similar stability and convergence as with the full Jacobian.

In addition to the time step or the CFL number, the space step of a grid cell plays an important role in the stability and convergence of the coupled implicit scheme. Eberhardt [7] and Kim [15] used different grid densities to numerically verify the stability of the FCI scheme and the accuracy of its numerical solutions. Glaz [17] used fine grids to analyze non-equilibrium effects in the oblique shock wave reflection region. Although it is known that better results are typically obtained using fine grids, there is no reasonable theoretical explanation about the relations between the space step and the stability of the numerical scheme.

In this paper, we investigate the full coupled implicit scheme for solving the governing equations about the inviscid chemical non-equilibrium flows and derive the corresponding amplification factor from Von Neumann stability theory. Stability analysis is performed on the stability of the FCI scheme with the full and the diagonalized Jacobians. And the effects of several factors (flow condition, CFL number, space step) are studied. Especially, the effect of the space step on the stability of the FCI scheme with the diagonalized Jacobian is discussed in detail. And an improved method on the grid distribution according to the flow conditions is proposed. Finally, some numerical tests are given to verify the aforementioned conclusions.

2 Governing equations

The conservation form of the two-dimensional Euler equations for chemical non-equilibrium flows with n species can be written in Cartesian coordinates as follows:

$$\frac{\partial \boldsymbol{Q}}{\partial t}+\frac{\partial \boldsymbol{F}}{\partial x}+\frac{\partial \boldsymbol{G}}{\partial y}=\boldsymbol{W}, \tag{2.1}$$

here $\boldsymbol{Q}$ is the vector of conservation variables, $\boldsymbol{F}$ and $\boldsymbol{G}$ are the vectors of the convective fluxes in the x- and y- directions, respectively, and $\boldsymbol{W}$ is a vector of the chemical source

term. The vectors $\boldsymbol{Q}$, $\boldsymbol{F}$, $\boldsymbol{G}$ and $\boldsymbol{W}$ are illustrated below:

$$\boldsymbol{Q}=\begin{bmatrix}\rho_s\\ \rho u\\ \rho u\\ \rho E\end{bmatrix},\quad \boldsymbol{F}=\begin{bmatrix}\rho_s u\\ \rho u^2+p\\ \rho uv\\ \rho uH\end{bmatrix},\quad \boldsymbol{G}=\begin{bmatrix}\rho_s v\\ \rho uv\\ \rho v^2+p\\ \rho vH\end{bmatrix},\quad \boldsymbol{W}=\begin{bmatrix}\dot{\omega}_s\\ 0\\ 0\\ 0\end{bmatrix},$$

with $s=1,\cdots,n$.

In general, the system is closed by state relations (e.g., $p=p(\rho,T)$ and $e=e(\rho,T)$).

The variable $\dot{\omega}_s$ in the vector is defined as the net mass production rate of the species s and is written as follows:

$$\dot{\omega}_s=M_s\sum_{k=1}^{NR}(\dot{C}_s)_k, \tag{2.2}$$

where NR is the total number of reactions, and $(\dot{C}_s)_k$ is the rate of production of moles of species s by reaction k,

$$(\dot{C}_s)_k=(\beta_{sk}-\alpha_{sk})\left[k_{fk}\prod_{m=1}^{n}(C_m)^{\alpha_{sk}}-k_{bk}\prod_{m=1}^{n}(C_m)^{\beta_{sk}}\right],$$

where the kth reaction is written as follows:

$$\sum_{s=1}^{n}\alpha_{sk}[M]_s\underset{k_{bk}}{\overset{k_{fk}}{\Longleftrightarrow}}\sum_{s=1}^{n}\beta_{sk}[M]_s.$$

Here, $[M]_s$ represents species s, α_{sk} and β_{sk} are the stoichiometric coefficients for the species s in the kth reaction, k_{fk} and k_{bk} are the forward and backward reaction rates, respectively, and M_s is the molecular weight of the species s. C_s is the molar concentration of the species and is given by $C_s=\rho_s/M_s$.

For the convenience in the analysis, we consider a simple chemical model with two species: N_2 and N. The chemical reactions are the dissociation and recombination reactions of the two species and are shown below [18]:

$$N_2+N_2\Longleftrightarrow 2N+N_2, \tag{2.3a}$$

$$N_2+N\Longleftrightarrow 2N+N. \tag{2.3b}$$

3 Numerical methods

3.1 Fully coupled implicit scheme

The non-equilibrium system itself is a strongly coupled system of gas dynamic equations and species equations. Thus, the FCI scheme based on FVM is used to solve Eq. (2.1).

The time derivative terms of Eq. (2.1) are replaced by a first-order backward difference, and the implicit convective flux and the chemical source term are handled using

the linearized approximate method and the flux vector splitting technique. The numerical scheme of Eq. (2.1) can be written as follows:

$$(\boldsymbol{L}+\boldsymbol{D}+\boldsymbol{U})\Delta\boldsymbol{Q}^n=\boldsymbol{RHS}, \tag{3.1}$$

where $\boldsymbol{D}$ is a block diagonal matrix, $\boldsymbol{L}$ is a block lower triangular matrix, $\boldsymbol{U}$ is a block upper triangular matrix, and $\boldsymbol{RHS}$ is a right-hand-side residual.

Many iterative methods are available to approximately solve a system of linear equations, such as the alternating-direction-implicit method (ADI) [19], the lower-upper symmetric Gauss-Seidel method (LU-SGS) [20], etc. Considering the better stability of the LU-SGS method, this method is adopted in this paper. Thus, Eq. (3.1) is rewritten as follows:

$$(\boldsymbol{D}+\boldsymbol{L})\boldsymbol{D}^{-1}(\boldsymbol{D}+\boldsymbol{U})\Delta\boldsymbol{Q}^n=\boldsymbol{RHS}, \tag{3.2}$$

where

$$\boldsymbol{D}\Delta\boldsymbol{Q}^n=\left\{\left(\frac{V_{i,j}}{\Delta t}+\rho(\boldsymbol{A}_{i,j})S_I+\rho(\boldsymbol{B}_{i,j})S_J\right)\boldsymbol{I}-\boldsymbol{Z}_{i,j}V_{i,j}\right\}\Delta\boldsymbol{Q}^n_{i,j}, \tag{3.3a}$$

$$\boldsymbol{L}\Delta\boldsymbol{Q}^n=-\boldsymbol{A}^+_{i-1/2,j}S_{i-1/2,j}\Delta\boldsymbol{Q}^n_{i-1,j}-\boldsymbol{B}^+_{i,j-1/2}S_{i,j-1/2}\Delta\boldsymbol{Q}^n_{i,j-1}, \tag{3.3b}$$

$$\boldsymbol{U}\Delta\boldsymbol{Q}^n=\boldsymbol{A}^-_{i+1/2,j}S_{i+1/2,j}\Delta\boldsymbol{Q}^n_{i+1,j}+\boldsymbol{B}^-_{i,j+1/2}S_{i,j+1/2}\Delta\boldsymbol{Q}^n_{i,j+1}, \tag{3.3c}$$

$$\begin{aligned}\boldsymbol{RHS}=&-\left(\tilde{\boldsymbol{F}}^n_{i+1/2,j}S_{i+1/2,j}-\tilde{\boldsymbol{F}}^n_{i-1/2,j}S_{i-1/2,j}+\tilde{\boldsymbol{G}}^n_{i,j+1/2}S_{i,j+1/2}-\tilde{\boldsymbol{G}}^n_{i,j-1/2}S_{i,j-1/2}\right)\\&+\boldsymbol{W}^n_{i,j}V_{i,j},\end{aligned} \tag{3.3d}$$

with

$$\Delta\boldsymbol{Q}^n_{i,j}=\boldsymbol{Q}^{n+1}_{i,j}-\boldsymbol{Q}^n_{i,j},\quad \tilde{\boldsymbol{F}}=\boldsymbol{F}n_{i,x}+\boldsymbol{G}n_{i,y},\quad \tilde{\boldsymbol{G}}=\boldsymbol{F}n_{j,x}+\boldsymbol{G}n_{j,y},$$

where $\boldsymbol{n}_i=(n_{i,x},n_{i,y})$ and $\boldsymbol{n}_j=(n_{j,x},n_{j,y})$ are the unit normal vectors of the interface in the i and j directions. $V_{i,j}$ and $S_{i+1/2,j}$ denote the volume and the interfacial area of a grid cell, respectively.

For simplicity, the discretization of Eq. (2.1) is based on a regular structured grid, i.e.,

$$S_I=\Delta y,\quad S_J=\Delta x. \tag{3.4}$$

Therefore, the time step Δt can be calculated as follows:

$$\Delta t=\frac{CFL}{\left[\frac{|u|}{\Delta x}+\frac{|v|}{\Delta y}+a\sqrt{\frac{1}{\Delta x^2}+\frac{1}{\Delta y^2}}\right]}. \tag{3.5}$$

And

$$\left.\begin{aligned}\boldsymbol{A}^\pm&=\frac{1}{2}\left[\boldsymbol{A}\pm\rho(\boldsymbol{A})\boldsymbol{I}\right]\\ \boldsymbol{B}^\pm&=\frac{1}{2}\left[\boldsymbol{B}\pm\rho(\boldsymbol{B})\boldsymbol{I}\right]\end{aligned}\right\}, \tag{3.6}$$

where $\boldsymbol{A}$ and $\boldsymbol{B}$ are the Jacobian matrices of $\tilde{\boldsymbol{F}}$ and $\tilde{\boldsymbol{G}}$, and $\boldsymbol{Z}$ is the Jacobian matrix of the chemical source term $\boldsymbol{W}$. Furthermore, $\rho(\boldsymbol{A})=\kappa\max[|\lambda(\boldsymbol{A})|]$, where κ is a parameter that is greater than or equal to unity.

In addition, the interface fluxes $\tilde{\boldsymbol{F}}$ and $\tilde{\boldsymbol{G}}$ in the $\boldsymbol{RHS}$ are calculated using the first order Roe [21] scheme, which shows upwind characteristics, i.e.,

$$\tilde{\boldsymbol{F}}_{i+1/2}=\frac{1}{2}\left[\tilde{\boldsymbol{F}}(\boldsymbol{Q}_i)+\tilde{\boldsymbol{F}}(\boldsymbol{Q}_{i+1})-|\boldsymbol{A}|_{i+1/2}(\boldsymbol{Q}_{i+1}-\boldsymbol{Q}_i)\right], \tag{3.7}$$

where

$$\boldsymbol{A}=\partial\tilde{\boldsymbol{F}}/\partial\boldsymbol{Q}=\boldsymbol{T}^{-1}\boldsymbol{\Lambda}\boldsymbol{T},\quad |\boldsymbol{A}|=\boldsymbol{T}^{-1}|\boldsymbol{\Lambda}|\boldsymbol{T}.$$

3.2 Diagonalized method for source term Jacobian

The block diagonal matrix $\boldsymbol{D}$ in Eq. (3.3a) becomes a scalar diagonal matrix in the absence of the chemical source term. Thus, the inversion of the block matrix $\boldsymbol{D}$ in Eq. (3.2) is avoided, which greatly reduces the amount of computation and memory space required. This result is a significant advantage of the LU-SGS method. When the chemical source term is considered, different methods can be used to diagonalize $\boldsymbol{Z}$, which is also called the full Jacobian, to maintain the advantages of the LU-SGS method. Among these methods [7,15,16], the diagonalized method developed by Eberhardt and Imlay [7] is adopted.

The full Jacobian $\boldsymbol{Z}$ is given as

$$\boldsymbol{Z}=\frac{\partial\boldsymbol{W}}{\partial\boldsymbol{Q}}=\begin{bmatrix} \frac{\partial\dot{\omega}_1}{\partial\rho_1} & \cdots & \frac{\partial\dot{\omega}_1}{\partial\rho_{ns}} & \frac{\partial\dot{\omega}_1}{\partial\rho u} & \frac{\partial\dot{\omega}_1}{\partial\rho v} & \frac{\partial\dot{\omega}_1}{\partial\rho E} \\ \vdots & \ddots & \vdots & \vdots & \vdots & \vdots \\ \frac{\partial\dot{\omega}_{ns}}{\partial\rho_1} & \cdots & \frac{\partial\dot{\omega}_{ns}}{\partial\rho_{ns}} & \frac{\partial\dot{\omega}_{ns}}{\partial\rho u} & \frac{\partial\dot{\omega}_{ns}}{\partial\rho v} & \frac{\partial\dot{\omega}_{ns}}{\partial\rho E} \\ \boldsymbol{0} & \boldsymbol{0} & \boldsymbol{0} & \boldsymbol{0} & \boldsymbol{0} & \boldsymbol{0} \end{bmatrix}. \tag{3.8}$$

In the diagonalization method, the full Jacobian $\boldsymbol{Z}$ is replaced by the following diagonalized Jacobian:

$$\tilde{\boldsymbol{Z}}=\begin{bmatrix} \frac{1}{\tau_1} & \boldsymbol{0} & 0 & 0 \\ \boldsymbol{0} & \ddots & \boldsymbol{0} & \vdots \\ 0 & \boldsymbol{0} & \frac{1}{\tau_{ns}} & 0 \\ \boldsymbol{0} & \cdots & \cdots & \boldsymbol{0} \end{bmatrix}, \tag{3.9}$$

where τ_s is the characteristic time scale for the production or reduction of species s, which is defined as

$$\frac{1}{\tau_s}=\beta\left[\sum_{l=1}^{ns}\left(\frac{\partial\dot{\omega}_s}{\partial\rho_l}\right)^2\right]^{1/2}, \tag{3.10}$$

where β is a relaxation parameter that is greater than one.

4 Von Neumann stability analysis

Von Neumann stability theory is an invaluable tool for assessing the stability and convergence of numerical schemes. Strictly speaking, the theory is only applicable to linear equations with constant coefficients and periodic boundary conditions. Thus, the nonlinear terms of Eq. (3.2) are first linearized, and the coefficient matrices must be frozen. Eq. (3.3) is rewritten as follows:

$$\boldsymbol{D}\Delta\boldsymbol{Q}^n=\left\{\left(\frac{V_{i,j}}{\Delta t}+\rho(\boldsymbol{A})\Delta y+\rho(\boldsymbol{B})\Delta x\right)\boldsymbol{I}-\boldsymbol{Z}V_{i,j}\right\}\Delta\boldsymbol{Q}^n_{i,j}, \tag{4.1a}$$

$$\boldsymbol{L}\Delta\boldsymbol{Q}^n=-\boldsymbol{A}^+\Delta y\Delta\boldsymbol{Q}^n_{i-1,j}-\boldsymbol{B}^+\Delta x\Delta\boldsymbol{Q}^n_{i,j-1}, \tag{4.1b}$$

$$\boldsymbol{U}\Delta\boldsymbol{Q}^n=\boldsymbol{A}^-\Delta y\Delta\boldsymbol{Q}^n_{i+1,j}+\boldsymbol{B}^-\Delta x\Delta\boldsymbol{Q}^n_{i,j+1}, \tag{4.1c}$$

$$\begin{aligned}\boldsymbol{RHS}=&-\left[\left(|\boldsymbol{A}|\boldsymbol{Q}^n_{i,j}+\boldsymbol{A}^-\boldsymbol{Q}^n_{i+1,j}-\boldsymbol{A}^+\boldsymbol{Q}^n_{i-1,j}\right)\Delta y\right]\\&-\left[\left(|\boldsymbol{B}|\boldsymbol{Q}^n_{i,j}+\boldsymbol{B}^-\boldsymbol{Q}^n_{i,j+1}-\boldsymbol{B}^+\boldsymbol{Q}^n_{i,j-1}\right)\Delta x\right]\\&+\boldsymbol{Z}\boldsymbol{Q}^n_{i,j}V_{i,j},\end{aligned} \tag{4.1d}$$

where the term $\boldsymbol{ZQ}$ in Eq. (4.1d) is derived from

$$\boldsymbol{W}\approx\frac{\partial\boldsymbol{W}}{\partial\boldsymbol{Q}}\boldsymbol{Q}=\boldsymbol{Z}\boldsymbol{Q}.$$

Periodic boundary conditions are assumed. A discrete and finite Fourier representation of $\boldsymbol{Q}^n_{i,j}$ is given as

$$\boldsymbol{Q}^n_{i,j}=\sum\hat{\boldsymbol{Q}}^n e^{I(i\theta_x+j\theta_y)}, \tag{4.2}$$

where the phase angles θ_x and θ_y vary over the range $(-\pi,\pi]$, and $\hat{\boldsymbol{Q}}$ denotes the amplitude vector.

Therefore, the Fourier symbols of the scheme given by Eqs. (3.2) and (4.1) are

$$(\hat{\boldsymbol{D}}+\hat{\boldsymbol{L}})\hat{\boldsymbol{D}}^{-1}(\hat{\boldsymbol{D}}+\hat{\boldsymbol{U}})\Delta\hat{\boldsymbol{Q}}^n=\widehat{\boldsymbol{RHS}}\hat{\boldsymbol{Q}}^n, \tag{4.3}$$

where

$$\hat{\boldsymbol{D}}=\left(V_{i,j}/\Delta t+\rho(\boldsymbol{A})\Delta y+\rho(\boldsymbol{B})\Delta x\right)\boldsymbol{I}-\boldsymbol{Z}V_{i,j}, \tag{4.4a}$$

$$\hat{\boldsymbol{L}}=-\boldsymbol{A}^+\Delta y\cos(\theta_x)-\boldsymbol{B}^+\Delta x\cos(\theta_y)+i(\boldsymbol{A}^+\Delta y\sin(\theta_x)+\boldsymbol{B}^+\Delta x\sin(\theta_y)), \tag{4.4b}$$

$$\hat{\boldsymbol{U}}=\boldsymbol{A}^-\Delta y\cos(\theta_x)+\boldsymbol{B}^-\Delta x\cos(\theta_y)+i(\boldsymbol{A}^-\Delta y\sin(\theta_x)+\boldsymbol{B}^-\Delta x\sin(\theta_y)), \tag{4.4c}$$

$$\begin{aligned}\widehat{\boldsymbol{RHS}}=&-\left[|\boldsymbol{A}|\Delta y(1-\cos(\theta_x))+|\boldsymbol{B}|\Delta x(1-\cos(\theta_y))+i\left(\boldsymbol{A}\Delta y\sin(\theta_x)+\boldsymbol{B}\Delta x\sin(\theta_y)\right)\right]\\&+\boldsymbol{Z}V_{i,j}.\end{aligned} \tag{4.4d}$$

Finally, the amplification matrix is

$$\boldsymbol{G}=\boldsymbol{I}+\left[(\hat{\boldsymbol{D}}+\hat{\boldsymbol{L}})\hat{\boldsymbol{D}}^{-1}(\hat{\boldsymbol{D}}+\hat{\boldsymbol{U}})\right]^{-1}\widehat{\boldsymbol{RHS}}, \tag{4.5}$$

Table 1: Data for two flow conditions behind the shock wave in hypersonic flow fields.

Flow Condition		Ma	P [atm]	T [K]	Mass fraction of species in chemical equilibrium (Y_{N_2},Y_N) [22]
Type 1 (SUPLTP)	Case 1	5	0.01	1000	1.0, 0.0
	Case 2	10	0.001	500	1.0, 0.0
Type 2 (SUBHTP)	Case 3	0.1	10	10000	0.09, 0.91
	Case 4	0.5	1	8000	0.175, 0.825

where $\hat{\boldsymbol{Q}}^{n+1} = \boldsymbol{G}\hat{\boldsymbol{Q}}^n$.

The stability of the numerical scheme is analyzed by investigating the eigenvalue of the amplification matrix $\boldsymbol{G}$, which describes the variation of solution between one time interval. Stability is guaranteed when the spectral radius of the amplification matrix $\max(|\lambda(\boldsymbol{G})|)$, namely amplification factor, is no more than one.

There are primarily two flow conditions behind the shock wave in hypersonic flow fields: a supersonic state at low temperature and pressure (SUPLTP) and a subsonic state at high temperature and pressure (SUBHTP). Stability analyses of the FCI scheme with the full and the diagonalized Jacobians are carried out for the two flow conditions, and the chemical model is shown in Section 2. The impact of the chemical reactions on the stability is analyzed in terms of two factors: the amplification factor, which is depends on the CFL number and the space step, and the stiffness. For convenience, two cases are considered for each flow condition, and the initial conditions are shown in Table 1.

4.1 Stability of FCI scheme with full Jacobian

For the present chemical non-equilibrium problem in one dimension, the stability results for the FCI scheme is presented here. Fig. 1 shows the relationship between the amplification factor and the CFL number based on different mass fractions of species for the four cases listed in Table 1. As shown in Fig. 1(a), the FCI scheme shows excellent stability in the given range of CFL number ($0.01 \leq CFL \leq 1000$) for the SUPLTP condition when the mass fractions of species N_2 are 1.0 and 0.99. That is, the chemical reactions in non-equilibrium flows are primarily dissociation reactions or weak recombination reactions. When strong recombination reactions are dominant in non-equilibrium flows, such as the flow conditions in which the mass fraction of species is 0.8 in Fig. 1(a), the FCI scheme is conditionally stable. However, the maximum CFL number that satisfies the stability is still rather large and acceptable. Furthermore, the damping behavior of the FCI scheme with different CFL numbers is also shown in Fig. 1(b) for the SUPLTP conditions. A maximum CFL number of 40 is obtained for Case 1 in which the mass fraction of species is 0.8. If the CFL number was increased to 50, for example, the damping behavior would not improve for almost all of the frequency modes, and more significantly, the amplification factor would exceed unity for the low frequency modes. The same situation also occurs in the case 2.

For the SUBHTP condition, the stability characteristics of the FCI scheme with the full Jacobian are similar to those for the SUPLTP condition, as shown in Fig. 2(a). However,

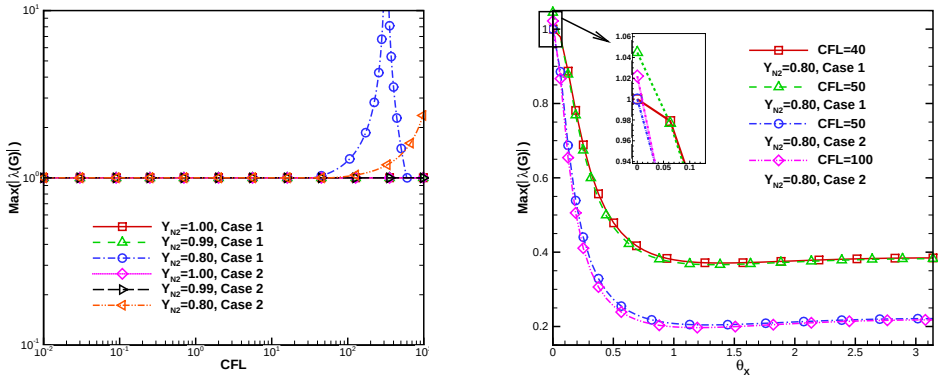

(a) (b)

Figure 1: One-dimensional stability of FCI scheme vs. CFL number (a) and phase angle (b) for the SUPLTP condition ($\Delta x = 0.01$).

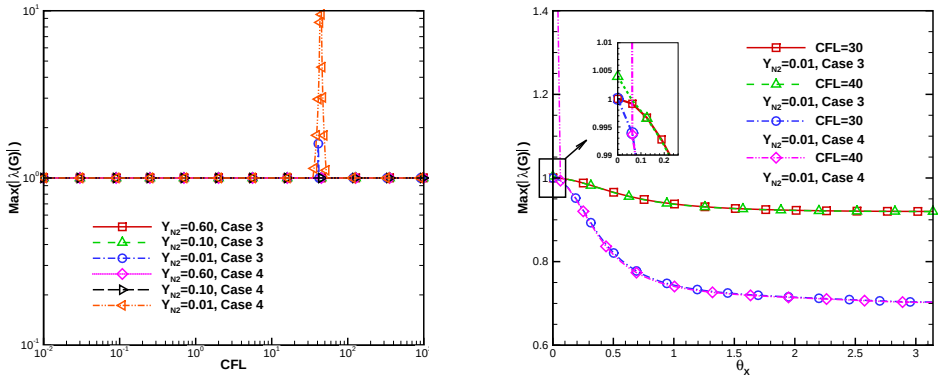

(a) (b)

Figure 2: One-dimensional stability of FCI scheme vs. CFL number (a) and phase angle (b) for the SUBHTP condition ($\Delta x = 0.01$).

in Fig. 2(b), the amplification factors of any cases are considerably larger than those for the SUPLTP condition. It explains that the damping behavior of the FCI scheme for the SUBHTP condition is worse than that for the SUPLTP condition. With the comparison between the Fig. 1(b) and Fig. 2(b), the CFL number satisfying the stability is generally larger for the SUPLTP condition than that for the SUBHTP condition, which means that a larger CFL number is fail for the latter in numerical computation. For example, when the CFL number is 40, the FCI scheme is stable for the SUPLTP condition but unstable for the SUBHTP condition. Thus, we can infer that the SUBHTP flow condition becomes a major factor which impacts the stability of the FCI scheme.

The stiffness of the governing equations is also considered. With respect to chemical kinetics, the stiffness is defined as the ratio of the fluid dynamics time scale $\tau_f = \Delta x/(|U|+a)$ [6] to the chemical reaction time scale $\tau_c = 1/\max(|\lambda(\boldsymbol{Z})|)$ [26] for non-

Table 2: Time scales and stiffnesses for two flow conditions.

	Y_{N_2}	τ_f	τ_c	τ_f/τ_c
Case 1	1.0	0.264e-5	0.101e15	0.263e-21
	0.99	0.262e-5	0.251	0.104e-4
	0.8	0.235e-5	0.293e-3	0.800e-2
Case 2	1.0	0.200e-5	0.178e18	0.113e-22
	0.99	0.199e-5	0.215e1	0.927e-6
	0.8	0.179e-5	0.132e-2	0.135e-2
Case 3	0.6	0.374e-5	0.129e-7	0.288e3
	0.1	0.300e-5	0.321e-7	0.935e2
	0.01	0.290e-5	0.724e-7	0.400e2
Case 4	0.6	0.306e-5	0.786e-6	0.390e1
	0.1	0.246e-5	0.191e-5	0.129e1
	0.01	0.238e-5	0.416e-5	0.572

equilibrium problems. Table 2 shows the two time scales and stiffness parameters which are calculated for the four cases listed in Table 1. For the SUPLTP condition, there is no stiffness because the ratio is very small, whereas in the SUBHTP condition, a large ratio yields a significant stiffness. Thus, the CFL number must be very small to avoid a non-physical solution or computational divergence. We conclude from the stability analyses above that the instability resulting from the stiffness can be greatly weakened or even eliminated if the numerical computation is carried out using the FCI scheme, and the CFL number can be ramped up to large value without a loss in stability.

We also briefly discuss the two-dimensional stability of the FCI scheme. Figs. 3(a) and (b) separately show the damping behavior of the FCI scheme for Case 2 and Case 3. Similar to the one-dimensional results which are shown in Fig. 1(a) and Fig. 2(a), the two-

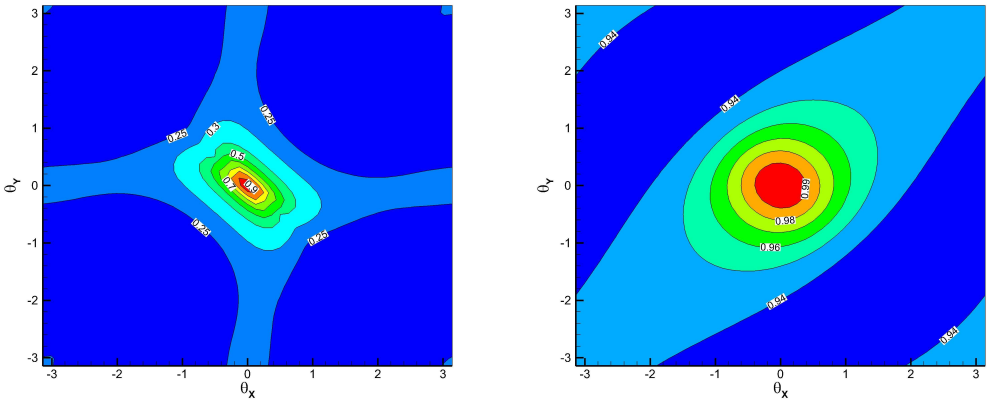

(a) Case 2, $Y_{N_2}=0.99$ (b) Case 3, $Y_{N_2}=0.6$

Figure 3: Contours of two-dimensional amplification factor of FCI scheme for Case 2 and Case 3 ($\Delta x=0.01$, $\Delta y=0.01$, $CFL=100$).

dimensional stability characteristic can also be satisfied for large CFL numbers. Meanwhile, the amplification factor under any pair of phase angles for the SUBHTP condition is much larger than that for the SUPLTP condition, which means that the damping behavior for the former is worse than that for the latter. This also explains that the former convergent rate is much smaller and will becomes major factor impacting the convergence of the FCI scheme. To summarize, the conclusions from the one-dimensional cases are also suitable for the two-dimensional cases.

4.2 Stability of FCI scheme with diagonalized Jacobian

Currently, although the diagonalization method is used to replace the full Jacobian, little research has been carried out on whether the inherent characteristics of the FCI scheme with the full Jacobian are maintained, that is, whether the numerical instability is weakened or even eliminated. Therefore, the stability of the FCI scheme with the diagonalized Jacobian $\tilde{\boldsymbol{Z}}$ is discussed in detail below. Although the parameter β is greater than one in [7], the numerical results in [23] show it is better to set the parameter β less than one. Thus, the relaxation parameter β is set to 0.5 in this paper.

Figs. 4(a) and (b) show the variations in the amplification factor of the FCI scheme with the diagonalized Jacobian based on different CFL numbers for the two flow conditions. Fig. 4(a) shows that for the SUPLTP condition, the range of CFL number that satisfy the stability for the diagonalized Jacobian is nearly invariant relative to that for the full Jacobian shown in Fig. 1(a). The FCI scheme exhibits similar damping behavior with the diagonalized Jacobian (not shown) as with the full Jacobian. However, for the SUBHTP condition, the stability characteristic of the FCI scheme with the diagonalized Jacobian is completely different from that with the full Jacobian. Fig. 4(b) shows that the diagonalization method seriously curtails the range of CFL number, which means that the numerical computation depends on a relatively small CFL number. Fig. 5 shows that

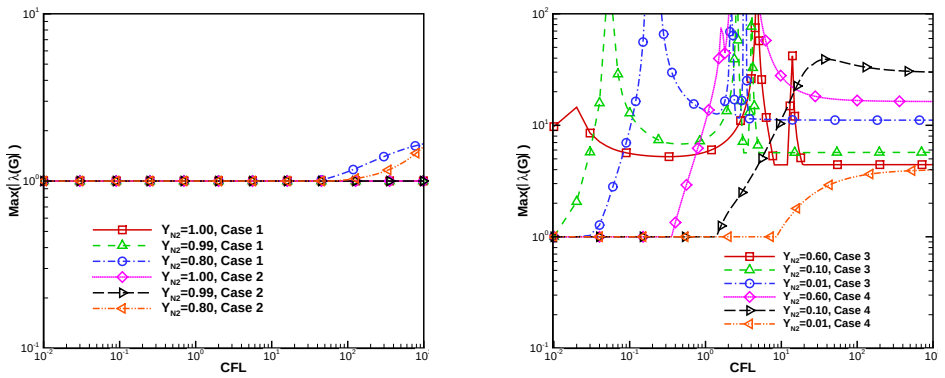

(a) (b)

Figure 4: One-dimensional stability of FCI scheme with diagonalized Jacobian (a) SUPLTP (b) SUBHTP ($\Delta x = 0.01$).

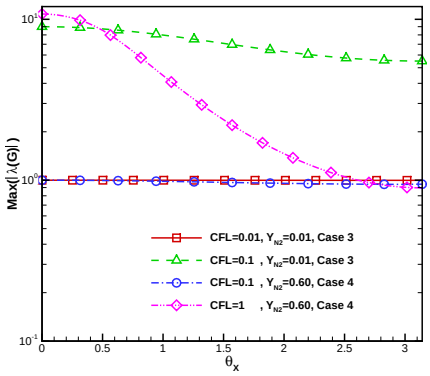

Figure 5: One-dimensional amplification factor of FCI scheme with diagonalized Jacobian vs. phase angle ($\Delta x = 0.01$).

for a larger CFL number, the damping behavior of the FCI scheme is destroyed for both the low and high frequency modes when the full Jacobian is diagonalized.

The analyses indicate that the FCI scheme with the diagonalized Jacobian does not maintain the excellent characteristics of the FCI scheme with the full Jacobian under certain circumstances, such as the SUBHTP condition or large space step, which explains why a large CFL number cannot be used in the FCI scheme with the diagonalized Jacobian. Similarly, these phenomena from the one-dimensional cases are also observed in the two-dimensional cases.

4.3 Effect of space step on stability

It is well known that the present FCI scheme is unconditionally stable in the absence of the chemical source term [20]. If the space step is very small, the $\boldsymbol{Z}V$ term in Eqs. (4.4a) and (4.4d) is close to zero, and the expression $\max(|\lambda(\boldsymbol{G})|) \leq 1$ probably should hold for any CFL number. In other word, we suppose that decreasing the space step can weaken the role of the Jacobian matrix of the chemical source term in the scheme. In previous studies, Eberhardt [7] and Dwight [13] achieved numerical convergence using grid refinement. Therefore, the effect of the space step on the stability of the FCI scheme with the diagonalized Jacobian is discussed in detail to solve the problems in Section 4.2.

In this section, stability analyses are performed for the SUBHTP condition in which the stiffness still exists and the CFL number is significantly limited. Here, three space steps are considered, as shown in Fig. 6(a). It is evident that decreasing the space step increases the maximum CFL number that satisfies the stability. And if the space step is reduced by one order of magnitude, the maximum CFL number increases by at least one order of magnitude. In addition, the damping behavior is also improved for a smaller space step, and a larger CFL number can be used, as shown in Fig. 6(b). Meanwhile, as the space step decreases, the FCI scheme with the diagonalized Jacobian shows similar stability characteristics to the full Jacobian, or even slightly better. Unfortunately, the

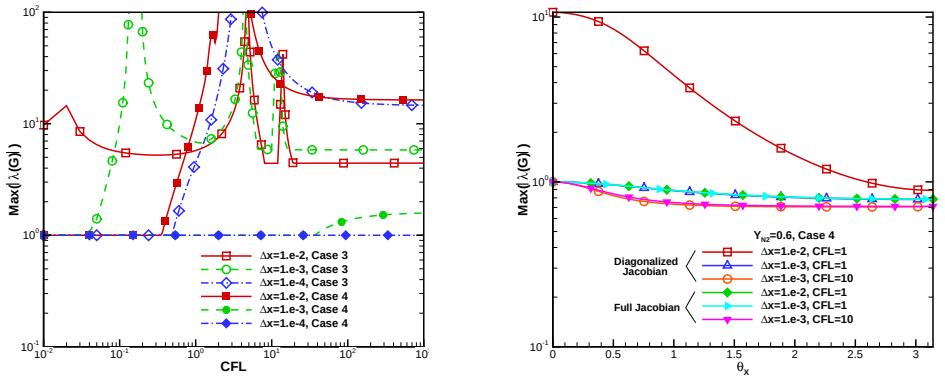

(a) (b)

Figure 6: Effect of space step on one-dimensional stability of FCI scheme with diagonalized Jacobian (a) CFL number (b) phase angle.

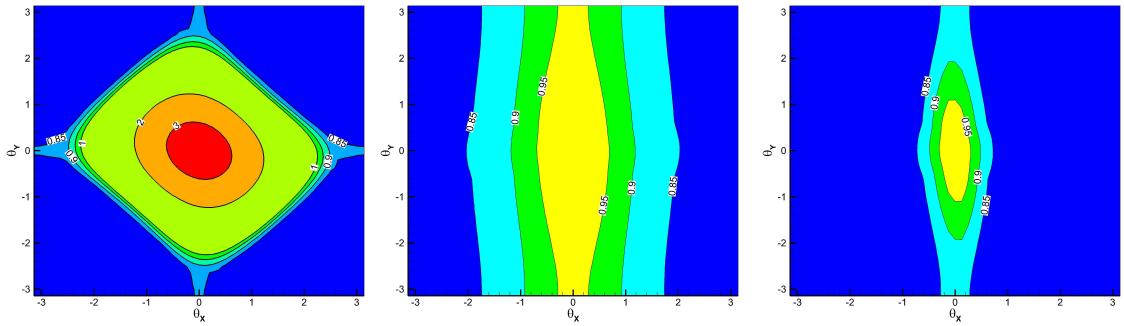

(a) $\Delta x=0.01$, $\Delta y=0.01$, $CFL=1$ (b) $\Delta x=0.001$, $\Delta y=0.01$, $CFL=1$ (c) $\Delta x=0.001$, $\Delta y=0.01$, $CFL=10$

Figure 7: Contours of two-dimensional amplification factor of FCI scheme with diagonalized Jacobian for Case 4 ($Y_{N_2}=0.6$).

damping rate is still relatively large.

Fig. 7 shows similar two-dimensional results for the SUBHTP condition. Fig. 7(a) shows that for a larger space step, the instability occurs for middle and low frequency modes and even for some high frequency modes. Fig. 7(b) shows that if the space step along the x-direction is reduced from 0.01 to 0.001, the instability vanishes, and the damping behavior along the x-direction is improved. Fig. 7(c) shows that increasing the maximum CFL number further improves the damping behavior.

In a word, the stability analyses verify the foregoing supposition. For the SUBHTP condition, the reduction of the space step can improve the stability of the FCI with the diagonalized Jacobian and increase the CFL number satisfying the stability. Therefore, a method for improving the stability, that the computational grid is refined locally based on the flow conditions, such as the SUBHTP condition, is suggested.

5 Numerical validation and discussions

To validate the stability and convergence analyses presented in Section 4, we first consider a steady two-dimensional hypersonic inviscid flow around a cylinder. The free stream Mach number is 10, and the static temperature is 700K [18]. The free stream conditions produce extremely high temperature in the region between the bow shock and the stagnation point, which promotes the nitrogen dissociation reactions.

At first an initial grid with 51×51 grid points, as shown in Fig. 8(a), is given. Fig. 10(a) shows the convergence histories of the FCI scheme with the full Jacobian for different CFL numbers based on the initial grid. The results illustrate that the stability and convergence of the scheme is not constrained by the CFL number. In addition, when the CFL number is greater than 100, the convergence is no longer improved, which agrees with the analyses in Section 4.1, where the damping behavior was no longer improved for excessively large CFL numbers.

However, Fig. 10(b) shows the convergence history of the FCI scheme with the diagonalized Jacobian based on the initial grid is poor for $CFL=5$. According to the foregoing stability analyses, and the fact that the region between the bow shock and stagnation point shows high temperature and subsonic state, the grid in the area of high temperature and subsonic state should be refined properly. Because of the characteristic of the thin shock layer for hypersonic flows, the refinement will not produce overmuch grid cells. At the same time, the grid in other regions can be coarse, such as the region in the front of the bow shock without chemical reactions, which will not destroy the stability and convergence of numerical computation. Therefore, an improved grid is exhibited in Fig. 8(b). Based on the improved grid, the FCI scheme with the diagonalized Jacobian

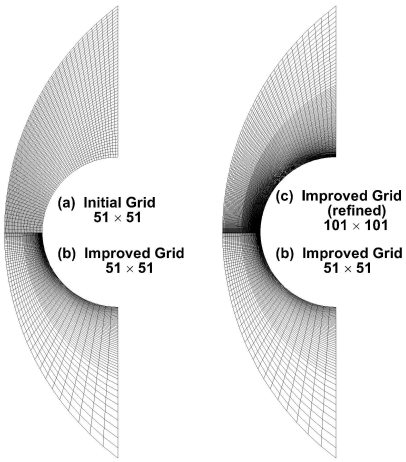

Figure 8: Initial and improved grids for a Mach 10 flow around a cylinder.

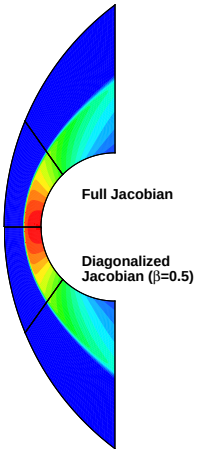

Figure 9: Comparison of pressure contours.

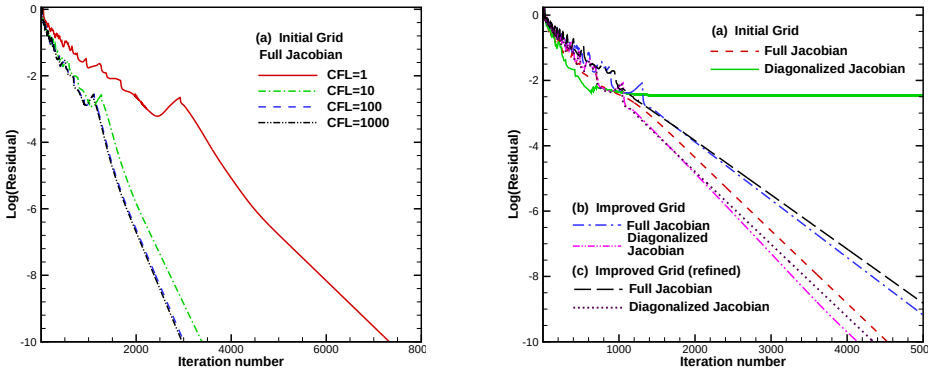

(a) (b) $CFL=5$

Figure 10: Convergence histories of the FCI scheme with full and diagonalized Jacobians ($\beta=0.5$).

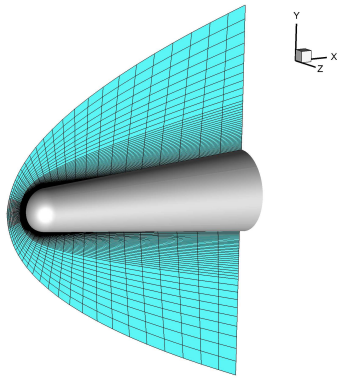

Figure 11: Improved grid for air reacting flow over the ELECTRE blunt cone.

shows good convergence for a large CFL number. And the comparison of pressure contours, which are obtained using two different Jacobians, is consistent, as shown in Fig. 9. Moreover, when the improved grid is refined in Fig. 8(c), the convergence histories show little change, as can be observed clearly in Fig. 10(b).

In addition, we can extend the above analyses to the problems involving more species and three dimension. Thus, An inviscid five-species air flow over ELECTRE blunt cone [24] with a Mach number of 13 is considered. Fig. 11 shows the improved grid while the initial grid is no longer given here. According to the residuals shown in Fig. 12, if the diagonalized Jacobian is selected in the FCI scheme based on the initial grid, the CFL number larger than 5 results in the nonphysical solutions. The problem is resolved by using the improved grid. The CFL number can be set to 50 or even greater. Finally, from the residuals of the two numerical tests, we obtain that the FCI scheme with the diagonalized Jacobian can exhibit similar stability and convergence characteristics to that with the full Jacobian for large CFL number based on the improved grid.

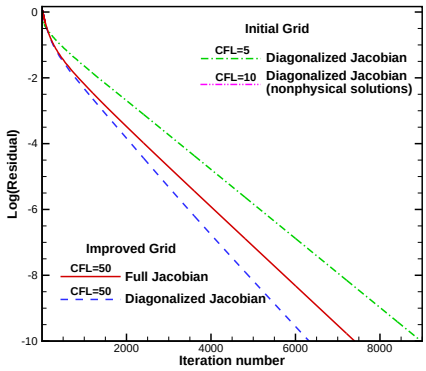

Figure 12: Convergence histories of the FCI scheme with full and diagonalized Jacobians ($\beta=0.5$).

6 Conclusions

Stability analyses of the fully coupled implicit scheme are carried out for the inviscid chemical non-equilibrium flows. The stability of the FCI scheme with the full Jacobian is related with the type of chemical reactions in flow field. It is regarded approximately as unconditionally stable for the dissociation reactions or the weak recombination reactions but is conditionally stable for the strong recombination reactions. However, for the latter, the maximum CFL number satisfying the stability is great enough and demonstrated to be optimal from the perspective of the amplification factor. Moreover, the instability, which results from the stiffness, is primarily encountered in the subsonic high-temperature region of flow fields, and can be weakened or even eliminated by the FCI scheme with the full Jacobian.

When the full Jacobian of chemical source term is replaced by the diagonalized Jacobian, the inherent characteristics of the FCI scheme vanish. The stability of the FCI scheme with the diagonalized Jacobian is sensitive to both the flow conditions and the space step. For the steady chemical non-equilibrium flow, a very small CFL number is required to guarantee computational convergence. In addition, the reduction of the space step can improve the stability of the FCI with the diagonalized Jacobian. Therefore, the paper presents a local grid refinement method according to the flow conditions.

The numerical tests further validate the theoretical analyses. The results show that the FCI scheme with the full Jacobian is hardly influenced by the CFL number, and shows good adaptability to a general grid. While the FCI scheme with the diagonalized Jacobian relies heavily on the CFL number. After the grid is refined properly in the region of high temperature and subsonic state, the stability and convergence of the FCI scheme with the diagonalized Jacobian are improved, so that the CFL number can be ramped to rather large values. In a word, the proposed method in this paper contributes to improving the stability of the FCI scheme with the diagonalized Jacobian, and increasing the CFL number to enhance the convergence efficiency. More importantly, the stability analyses

can also provide a theoretical basis for us in numerical computation.

References

[1] J. D. ANDERSON, Hypersonic and High Temperature Gas Dynamics, McGraw-Hill Book Company, New York, 1989.

[2] T. L. CHIANG AND K. HOFFMANN, *Determination of computational time step for chemically reacting flows,* AIAA paper 89-1855, 1989.

[3] C. P. LI, *Chemistry split techniques for viscous reactive blunt body flow computations,* AIAA paper 87-0282, 1987.

[4] C. P. LI, *Computational aspects of chemically reacting flows,* AIAA-91-1574-CP, 1991.

[5] M. E. OLSEN, D. K. PRABHU AND T. OLSEN, *Implementation of finite rate chemistry capability in overflow*, AIAA paper 04-2372, 2004.

[6] T. R. BUSSING AND E. M. MURMAN, *Finite volume method for the calculation of compressible chemically reacting flows*, AIAA J., 26 (1988), pp. 1070–1078.

[7] S. EBERHARDT AND S. IMLAY, *Diagonal implicit scheme for computing flows with finite rate chemistry,* J. Thermophys. Heat Transfer, 6 (1992), pp. 208–216.

[8] G. CANDLER AND R. W. MACCORMACK, *The computation of hypersonic ionized flow in chemical and thermal non-equilibrium,* AIAA paper 88-0511, 1988.

[9] S. C. SPIEGEL, D. L. STEFANSKI, H. LUO AND J. R. EDWARDS, *A cell-centered finite volume method for chemically reacting flows on hybrid grids,* AIAA paper 10-1083, 2010.

[10] S. C. SPIEGEL, D. L. STEFANSKI, H. LUO AND J. R. EDWARDS, *A regionally structured/ unstructured finite volume method for chemically reacting flows,* AIAA paper 11-3048, 2011.

[11] J. D. LAMBERT, Computational Methods in Ordinary Differential Equations, John Wiley & Sons, 1973.

[12] J. K. FASSBENDER, Improved Robustness for Numerical Simulation of Turbulent Flows around Civil Transport Aircraft at Flight Reynolds Numbers, Ph.D. Dissertation, Institute of Aerodynamics and Flow Technology, DLR, Brauschweig, 2003.

[13] R. P. DWIGHT, Efficiency Improvements of RANS-Based Analysis and Optimization Using Implicit and Adjoint Methods on Unstructured Grids, Ph.D. Dissertation, School of Mathematics, University of Manchester, 2006.

[14] S. VENKATESWARAN AND O. MICHAEL, *Stability analysis of fully coupled and loosely coupled schemes for combustion CFD,* AIAA paper 03-3543, 2003.

[15] S. L. KIM, I. S. JEUNG, Y. H. PARK AND J. Y. CHOI, *Approximate Jacobian methods for efficient calculation of reactive flows,* AIAA paper 00-3384, 2000.

[16] Y. JU, *Lower-upper scheme for chemically reacting flow with finite rate chemistry,* AIAA J., 33 (1995), pp. 1418–1425.

[17] H. GLAZ AND P. COLELLA, *Non-equilibrium effects in oblique shock wave reflection,* AIAA J., 26 (1985), pp. 46–53.

[18] R. J. GOLLAN, *Yet another finite-rate chemistry module for compressible flow codes,* Division Report, 9 (2003).

[19] R. M. BEAM AND R. F. WARMING, *An implicit finite difference algorithm for hyperbolic system in conservation law form,* J. Comput. Phys., 22 (1976), pp. 87–109.

[20] S. YOON AND A. JAMESON, *Lower-upper symmetric-gauss-sediel method for the Euler and Navier-Stoker equations,* AIAA J., 26 (1988), pp. 1025–1026.

[21] P. L. ROE, *Approximate Riemann solvers, parameter vectors and difference schemes,* J. Comput. Phys., 43 (1981), pp. 357–372.
[22] S. GORDON AND B. J. MCBRIDE, *Computer program for calculation of complex chemical equilibrium compositions and alpplications: I Analysis,* NASA Reference Publication 1311, NASA, 1994.
[23] B. HASSAN, G. V. CANDLER AND D. R. OLYNICK, *Thermo-chemical nonequilibrium effects on the aerothermodynamics of aerobraking vehicles,* J. Spacecraft Rockets, 30 (1993), pp. 647–655.
[24] J. MUYLAERT, L. WALPOT AND J. HAUSER, *Standard model testing in the european high enthalpy facility F4 and extrapolation to flight,* AIAA paper 92-3905, 1992.
[25] B. CHEN, L. WANG AND X. XU, *An implicit upwind parabolized Navier-Stokes code for chemically non-equilibrium flows,* Acta Mech. Sinica, 29 (2013), pp. 36–47.
[26] Y. G. BIAN AND L. G. XU, Aerothermodynamics (Second Edition), Press of University of Science and Technology of China, He Fei, 2011.